Recent Progress Towards Developing an Insect-Inspired Flapping-Wing Micro Air Vehicle

K. Knowles, S. A. Ansari, P. C. Wilkins, R. W. Zbikowski
Department of Aerospace, Power and Sensors
Cranfield University
Defence Academy of the United Kingdom
Shrivenham, SN6 8LA. UK

K.Knowles@cranfield.ac.uk

ABSTRACT

This paper presents an overview of the on-going research activities at Shrivenham, aimed at the design of an autonomous flapping-wing micro air vehicle. After introducing the problem of insect wing kinematics and aerodynamics, we describe our quasi-three-dimensional aerodynamic model for flapping wings. This is followed by a brief discussion of some aerodynamic issues relating to the lift-generating leading-edge vortex. New results are then presented on modelling of wing aeroelastic deflections. Finally, some brief observations are made on flight control requirements for an insect-inspired flapping-wing micro air vehicle. Overall, it is shown that successful development of such a vehicle will require a multi-disciplinary approach, with significant developments in a number of disciplines. Progress to date has largely been concerned with hover. Little is known about the requirements for successful manoeuvre.

1.0 INTRODUCTION

Agile flight inside buildings, caves and tunnels is of significant military and civilian value. Current surveillance assets (e.g. satellites, UAVs) possess virtually no capabilities of information-gathering inside buildings. The focus on indoor flight leads to the requirement of a distinct flight envelope. In addition, autonomy is required to enable mission-completion without the assistance of a human telepilot; this requires precise flight control. Current unmanned aerial vehicles (UAVs) are too large to achieve indoor flight and our research has concluded (see Refs [1][2][3]) that insect-like flapping flight is the optimum way to fulfil this capability — fixed wing aircraft do not have the required low-speed agility and miniature helicopters are too inefficient and noisy. Insect flapping flight, on the other hand, has been present in nature for over 300 million years [4] and has been perfected over this time. Insects fly at low speeds, are extremely manoeuvrable, virtually silent and most are capable of hover. In addition, insect flapping flight also offers significantly better power efficiency, particularly at low flight speeds, than both fixed-wing aircraft and rotorcraft [5][6], making it ideal for our focus on micro UAVs for indoor flight.

Cranfield University at Shrivenham, together with our partners in other universities (currently Oxford, Heriot-Watt and Bristol) are engaged in world-leading research on flapping-wing micro air vehicles (FMAVs), based on insect-like aerodynamics. A micro air vehicle is defined here as a hand-sized flying machine having no dimensions greater than ca. 15cm. This paper will review our key work to date. The paper is organised as follows. First, the flapping-wing problem is introduced by familiarising the reader with insect flight kinematics and relevant aerodynamic phenomena. Then, a brief description of our aerodynamic model is presented. This is followed by discussion of some relevant aerodynamic phenomena which are not directly captured in this model. We next discuss some recent findings on aeroelasticity before finally highlighting some considerations for flight control of an FMAV.

Knowles, K.; Ansari, S.A.; Wilkins, P.C.; Zbikowski, R.W. (2007) Recent Progress Towards Developing an Insect-Inspired Flapping-Wing Micro Air Vehicle. In *Platform Innovations and System Integration for Unmanned Air, Land and Sea Vehicles (AVT-SCI Joint Symposium)* (pp. 35-1 – 35-12). Meeting Proceedings RTO-MP-AVT-146, Paper 35. Neuilly-sur-Seine, France: RTO. Available from: http://www.rto.nato.int/abstracts.asp.

2.0 FLAPPING-WING PROBLEM

Understanding the flapping flight of insects has long been elusive due to the high forces generated that cannot be explained by conventional aerodynamics. For the development of an engineering model to demonstrate the behaviour of such flapping wings, therefore, it is necessary first to understand the underlying kinematics responsible for the forces and the associated aerodynamics. Wing kinematics encompass a whole series of design parameters that can be optimised to give the desired performance, once their effects are quantified.

2.1 Kinematics

The availability of high-speed photography has enabled reasonably good descriptions of the kinematics of insect wings [7][8][9]. Insects have either one or two pairs of wings. We restrict ourselves to one pair of wings (diptera) and the description that follows is for such an insect. The overall flapping motion is similar to the sculling motion of the oars on a rowboat, consisting essentially of three component motions — sweeping (fore and aft motion), heaving (up and down motion) and pitching (varying incidence). Flapping frequency is typically in the range 5–200 Hz. The wing motion can be divided broadly into two phases — translational and rotational. The translational phase consists of two half-strokes — the downstroke and the upstroke (see Figure 1). The downstroke refers to the motion of the wing from its rearmost position to its foremost position, relative to the body. The upstroke describes the return cycle. At either end of the half-strokes, the rotational phases come into play — stroke reversal occurs, whereby the wing rotates rapidly and reverses direction for the subsequent half-stroke. During this process, the morphological lower surface becomes the upper surface and the leading edge always leads (Figure 1a).

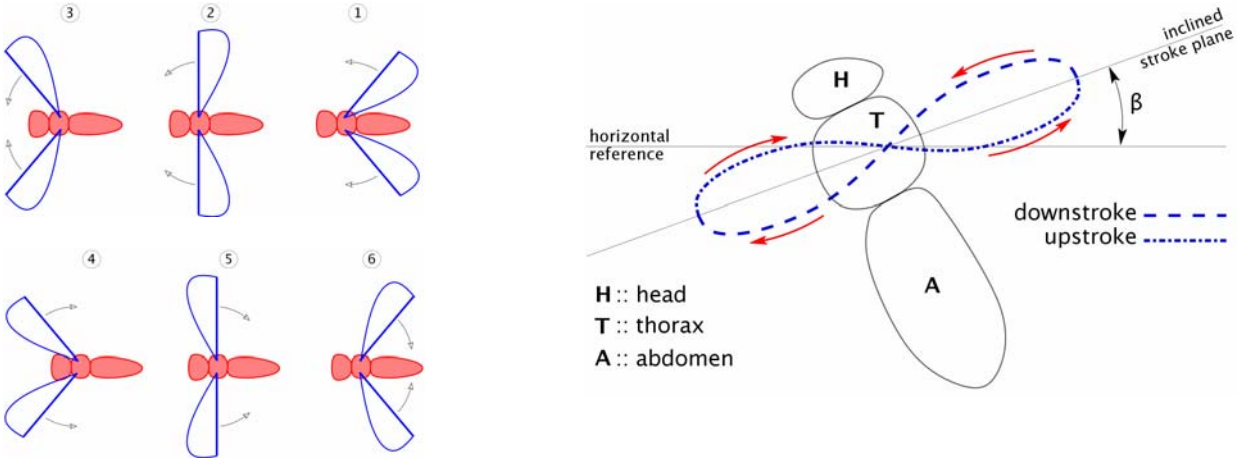

Figure 1: Insect-like flapping: (a) top view, showing downstroke (1-3) and upstroke (4-6) (left); (b) side view (right)

The path traced out by the wing tip (relative to the body) during the wing stroke is similar to a figure-of-eight on a spherical surface (see Figure 1b) as the wing semi-span is constant. The wing flaps back and forth about a roughly constant plane called the stroke plane (analogous to the tip-path-plane for rotorcraft). The stroke plane is inclined to the horizontal at the stroke-plane angle β (Figure 1b). The angle swept by the wing during a half-stroke is the stroke amplitude φ. During a half-stroke, the wing accelerates to a roughly constant speed around the middle of the half-stroke, before slowing down to rest at the end of it. The velocity during the wingbeat cycle is, therefore, non-uniform and for hover, in particular, the motion of the wing tip does not vary dramatically from a pure sinusoid [7]. Wing pitch also changes during the half-stroke, generally increasing gradually as the half-stroke proceeds. The maximum pitch angle of 90^{o} will occur near the ends of each half-stroke. A maximum pitch before the wing comes to rest is referred to

here as pitch advance, whereas a maximum pitch after the start of the next half-stroke is pitch delay

2.2 Aerodynamics

The flow associated with insect flapping flight (and scales pertaining to micro UAVs) is incompressible, laminar, unsteady and occurs at low Reynolds numbers. Despite their short stroke lengths and small Reynolds numbers, insect wings generate forces much higher than their quasi-steady equivalents due to the presence of a number of unsteady aerodynamic effects. The flow is now understood to comprise two components — attached and separated flow [10]. The attached flow refers to the freestream flow on the aerofoil as well as that due to its unsteady motion (sweeping, heaving and pitching). For insect-like flapping wings, flow separation is usually observed at both leading and trailing edges — the leading-edge vortex (LEV), which is bound to the wing for most of the duration of each half-stroke, and the trailing-edge wake, that leaves smoothly off the trailing edge. Flow is more or less attached in the remaining regions of the wing. The leading-edge vortex is believed to be responsible for the augmented forces observed [11][12].

3.0 AERODYNAMIC MODELLING

As part of our study of insect-like flapping flight, a nonlinear, unsteady aerodynamic model [14] has been developed to simulate this flow regime [15][16]; for full details see Ansari (2004)[13]. The model is inviscid and quasi-three-dimensional, and yet, shows remarkable agreement with existing experimental data, both in terms of force prediction and flowfield representation (see below). Consequently, it has proved to be a valuable design tool for flapping-wing problems. The simplicity of the model (due to its inviscid nature) makes it particularly useful for rapidly iterating through various wing configurations and designs, much faster than would a conventional Reynolds-averaged Navier-Stokes (RANS) CFD model. This model has been used for parametric studies [17] - showing, amongst other things, the importance of pitch advance in controlling lift. The model also gives insight into important flow phenomena.

3.1 Methodology

The model is quasi-three-dimensional; strip theory is used to divide the wing spanwise into chordwise sections that are each treated essentially as two-dimensional. Division of the wing into sections requires closer attention. The low aspect ratio and high solidity (the ratio of wing area to swept area) of insect wings requires that radial chords be used instead of normal (straight) chords (see Figure 2). This is necessary because each wing section would otherwise see a significant spanwise component of incident velocity, whose effect would be un-modelled. As a result, each wing section resides in a radial cross-plane that is then unwrapped flat and the flow is solved as a planar two-dimensional problem. The overall effect on the wing is obtained by integrating along the span.

The aerodynamics of flapping wings is realised using potential flow. As observed in insect flight, flow separates from both leading and trailing edges where the Kutta-Joukowksi condition is enforced. Further, the flow is assumed to be irrotational (except at solid boundaries and discontinuities in the wake). So in essence, the flow is solved for using Laplace's equation. Although viscosity is generally ignored, its effects are included indirectly in the form of the Kutta-Joukowksi condition and in the formation and shedding of vortices. The nature of Laplace's equation means that the principle of linear superposition can be applied — quasi-steady (wake-free) and unsteady (wake-induced) components are computed separately, and the net effect is obtained by taking their sum. The flow is solved for by satisfying the kinematic boundary conditions at the wing surface, the Kutta-Joukowski condition at the wake-inception points and by requiring that the total circulation in a control volume enclosing the system must remain constant (Kelvin's law). What finally results are two coupled, nonlinear, wake integral equations that together describe the flow in its entirety (within the limits of the assumptions made). Conformal

transformation is used and all calculations are performed in the circle plane.

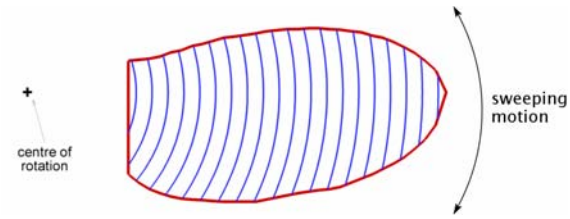

Figure 2: Radial chords used in aerodynamic modelling

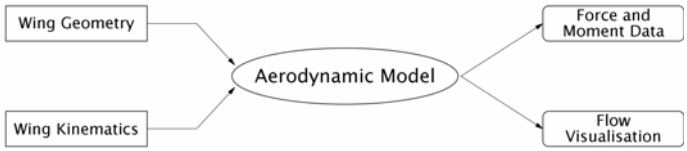

Figure 3: Data flow in the aerodynamic model

3.2 Implementation & Validation

The solution is implemented using the discrete point vortex method. The aerofoil in each 2-D section is represented by a distribution of bound vortices and the zero through-flow condition is enforced there. The two wakes shed from the leading and trailing edges are also distributions of vorticity but these are free to move with the fluid flow. At each time-step, the quasi-steady bound circulation is computed for smooth flow at the trailing edge. Two new vortices are then released, one each from the leading and trailing edges, and placed such that they follow the trace left by the previous vortex. The nonlinear equations referred to above are then solved simultaneously for the circulation strengths of the two new vortices. At the end of the time-step, the solution is marched forward in time by convecting the shed vortices in the wake using a forward Euler scheme. During the more acute phases of the flapping cycle (e.g. stroke reversals), the time-steps are subdivided into finer sub-time-steps to give better resolution but at the cost of increased CPU time. A spin-off of this method is that flow-visualisation is automatically generated (see Figures 3 & 4).

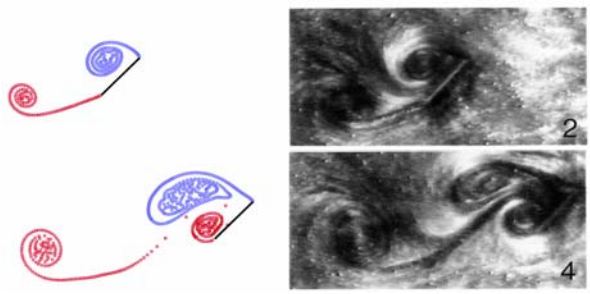

Figure 4: Comparison of flow visualisation for a wing after travelling 2 and 4 chord lengths: Cranfield's numerical predictions [16] (left) and benchmark experiments [19]

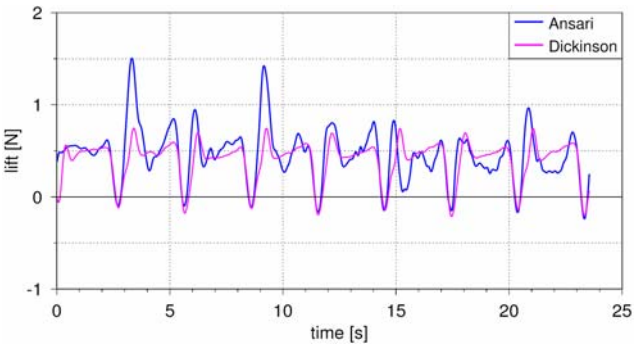

Figure 5: Lift force comparison: Cranfield's numerical predictions [16] and benchmark experiments [9].

Forces are computed by Kelvin's method of impulses [18]. The bound and shed vortices constitute vortex pairs that impart impulses between them. The combined time-rate-of-change of impulse of all vortex pairs is a measure of the force on the wing (since only the bound vortices sustain Kutta-Joukowski forces). Moment is computed similarly from the moment of impulse. In order to validate the model, predictions from it were compared with experimental results. Remarkable agreement was found both in terms of flowfield comparisons with Dickinson & Götz [19] (see Figure 4) as well as force comparisons (see Figure

5) with data provided by Dickinson from his Robofly experiments (see: [9]; [13]; [16]).

An important observation made during the development of the model was that flow behaviour is very strongly dependent on the number of chord lengths travelled. Flow in the outboard regions, having travelled more chord lengths, is more developed and 'older' in terms of chord lengths travelled. Therefore, it is more prone to vortex breakaway. A similar observation was made by Ellington et al. [11] and van den Berg & Ellington [20] from experiments using Ellington's flapper. They reported that, in the latter stages of the halfstroke, vortex breakdown caused the leading-edge vortex to 'lift off' the wing surface in these regions of the wing. New light is shed on this phenomenon in Section 4 below.

4.0 LEADING-EDGE VORTEX STABILITY

Details of the three-dimensional flow produced by a flapping wing are being investigated using RANS CFD [21]. Ansari's model is essentially inviscid, although the effects of viscosity are introduced 'artificially' by imposing separation at the leading and trailing edges of the aerofoil. Since FMAVs will operate at relatively low Reynolds numbers (~35000) at which viscous forces might be thought to be dominant, and since FMAV wings are known to experience three-dimensional flow effects, the accuracy of the model when compared to experimental data is surprising. The CFD research is investigating a number of issues related to this.

Insect wings operate at high angles of attack (>45^{o}), but instead of stall occurring, a stable, lift-enhancing LEV is created. It is likely that any FMAV will have to retain this phenomenon in order to retain the high efficiency of insect-like flapping. However, the reason or reasons for the stability of the LEV are still not entirely clear. The generally accepted view is that spanwise flow within the LEV extracts vorticity from it, meaning it does not grow to an unstable size [22]. Others have found no evidence of the spanwise flow and have instead postulated that the tip vortex is somehow responsible for limiting the LEV's growth [23]. More recently, some authors have suggested that the LEV is in fact unstable [24]. It appears that the stability of the LEV may be affected by Reynolds number, and since FMAVs will operate at higher Reynolds numbers than insects, it is important to investigate this effect.

In order to isolate 2D effects from 3D effects, we have first investigated the flow around 2D aerofoils at high angles of attack. This has shown that for Reynolds numbers of 25 or greater, any LEVs that appear are quickly shed, and their lift-enhancing effect is transient. At Reynolds numbers higher than 1000, Kelvin-Helmholtz instability (KHI) appears in the leading- and trailing-edge vortex sheets. However, this instability does not affect the frequency of the shedding of primary leading- and trailing-edge vortices; nor does the occurrence of KHI have a dramatic impact on the lift produced.

However, the 2D results also showed that the pressure at the core of an LEV decreases as the velocity of the flow is increased. This explains the spanwise flow that is seen in 3D cases - outer sections of the wing are moving faster and therefore generate an LEV with lower core pressure, leading to a spanwise pressure gradient. Spanwise flow occurs at all Reynolds numbers tested - the lowest being Re=120. The resulting LEV is stable even at Reynolds numbers of the order of 10000; although KHI does occur in the leading-edge vortex sheet, it does not cause the LEV to detach from the wing.

All of the CFD research so far has dealt with steady aerofoil or wing motion. The next stage will involve investigating the effects of aerofoil and wing acceleration.

5.0 AEROELASTIC EFFECTS

The authors and their co-investigators from Oxford University (Thomas, Taylor et al.) and Heriot-Watt University (Moore et al.) have recently completed a ground-breaking investigation of insect wing

aeroelasticity. The project integrated experimental and theoretical work to collect hitherto unavailable kinematic data for hovering insects in free flight. These data were used to develop a fundamental understanding of insect flight and to underpin novel dynamic modelling of flapping wings for use in the ongoing research programme to develop flapping-wing micro air vehicles at Cranfield University.

Hitherto, no reports exist in the literature of experimental data for insect-wing deformation at a dense grid of points during free flight. Some previous analysis has assumed that the wing behaves as a rigid plate [25] but this is inappropriate. Other workers have analysed the wing as a half-rigid plate [26], where the wing is divided into a number of chord-wise strips that can rotate independently about the longitudinal axis of the wing. The half-rigid model is not applicable to wings where chord deformation (camber) is significant. Wing camber measurements on free-flying [27] dragonflies were previously made using a stripe projection technique. This technique cannot be used, however, where the spar structure is too sparse for projected fringes to be visible, such as in hoverflies.

Dynamic modelling of insect wings aims to establish the nature of the observed deformation of insect wings: is the deformation predominantly due to inertial forces or aerodynamic forces, i.e. inertioelastic or aeroelastic in nature? Answering this question was hampered by the lack of detailed wing data, as explained above, and also by the lack of adequate aerodynamic modelling capabilities [28][29]. Our recent work has produced an aeroelastic model of wing deformation which couples our aerodynamic model (see Section 3) with an appropriate elasticity model of the insect wing (see Section 5.2) and new experimental data (see Section 5.1).

5.1 Experimental Work

Photogrammetric techniques were used by our partners at Heriot-Watt and Oxford Universities to measure insect wing deflections in flight. Initial measurements used locusts tethered on a 6-component force balance in the Oxford University low-speed, low-turbulence wind tunnel. These experiments allowed the optical instrumentation to be tested under near-ideal conditions. The locust wingbeat frequency is about 20Hz (similar to the target figure for an FMAV) making 1000 fps cameras and white light illumination suitable for image acquisition without image blur or overheating the insects. Wing position and incidence errors were found to be an order of magnitude smaller than for previous methods. Force balance measurements, wing weighing and laser vibrometer measurements were also included.

Measured points on wing veins were connected using cubic spline interpolation, and a mesh was fitted to reconstruct the wing surface. An empirical model of the mass distribution of the locust wing was fitted by cutting the wings into ca. 40 smaller pieces, and weighing these fresh. This was combined with the local acceleration data to estimate the local inertial forces acting on the wings, which were subtracted from the measured forces to calculate the aerodynamic forces.

The techniques developed with the locusts were applicable to the more difficult case of free-flying hoverflies, but white light could not be used with hoverflies because continuous illumination overheats the insects, whilst visible pulsed illumination alters the insects' natural wingbeat. For free-flight experiments, therefore, a 200W, 808nm, (infra-red and therefore invisible to the insects) pulsed diode laser was used [30] with a maximum pulse duration of 80μs and maximum repetition rate of 5kHz. The laser beam was focused on to a fibre array of four 2m lengths of plastic optical fibre. The output light from each of the 4 fibres was expanded through a 50.8mm focal length lens to produce four 60mm-diameter collimated beams that shone through the measurement volume into the lenses of four high-speed cameras.

The laser and cameras were operated in synchrony at 4kHz, yielding ca. 50 frames per wingbeat. The insect only triggered the cameras when it was hovering in the centre of the measurement volume. The same techniques as used with locusts were used to estimate the inertial forces.

The standard deviation of the 3D position errors was < 0.05mm in all axes. The shorter chord length for the hoverflies makes the angle of attack error roughly double that in locusts but still < 1°. The geometric angle of attack changes rapidly during the ends of the wingstrokes, but is then held fairly constant during the down- and upstrokes. The measurements reveal that the wings are not planar, with substantial twist from root to tip. There is also substantial camber throughout the wingstroke, and this is maintained during the translatory phase of the wingstrokes.

5.2 Mathematical Modelling

The complex kinematics of flapping result in deformation of insects' wings and the generation of lift . The elastic response of the wing is due to the interacting inertial and aerodynamic forces. As the wing beats, the aerodynamic force contributes to wing deformation, so the wing changes its shape, and this new shape modifies the aerodynamic force which, again, affects the wing's shape. This continuous and dynamic interaction between the elastic wing and the airflow is aeroelasticity. For flapping-wing aeroelasticity, the mathematical modelling has been divided into: (i) an aerodynamic model (see Section 3) and (ii) a structural model. The aeroelastic model was obtained by coupling (i) with (ii).

5.2.1 Elastic Model of Insect Wing

The structural model of the Eristalis wing must capture the wing's elasticity and be coupled with the aerodynamic model of Section 3. Since only flexural and torsional deflections need to be considered (at least for the experimental case of hoverflies), the Euler-Bernoulli beam model was sufficient to capture those deformations. In classical aeroelasticity [31] the emphasis is on modelling the Euler-Bernoulli beam with a partial differential equation (PDE), because for simple kinematics such a PDE admits solution by separation of variables. For insect flapping, the wing kinematics are highly non-uniform and the resulting PDE for flexural (bending) deflection $w = w(x, t)$ along the x-axis is:

$$\left[EIw''(x,t)\right]'' + m(x)\left\{\ddot{w}(x,t) - \left[\dot{\phi}^2(t)+\dot{\theta}^2(t)\right]w(x,t) + \left[\dot{\phi}(t)\dot{\psi}(t)-\ddot{\theta}(t)\right]x\right\} + \left[w'(x,t)\int_x^R m(\xi)\left\{-\left[\dot{\theta}^2(t)+\dot{\psi}^2(t)\right]\xi + \left[\dot{\phi}(t)\dot{\psi}(t)+\ddot{\theta}(t)\right]w(\xi,t) + 2\dot{\theta}(t)\dot{w}(\xi,t)\right\}\mathrm{d}\xi\right]' = 0 \qquad \text{Eqn (1)}$$

where φ, θ and ψ are the time-varying angles defining the wing kinematics, while dashes and dots represent spatial and temporal derivatives, respectively. Here, E is Young's modulus, I the area moment of inertia and R the beam length. This equation is much more complex than the recently considered case of non-uniform beam motion [32] and does not admit solution by separation of variables. The PDE for the torsional deflection is also involved and cannot be separated either.

A better strategy, well-suited to the wing-element nature of the aerodynamic model of Section 3, is to represent the Euler-Bernoulli beam in the lumped-parameter form [33]. This is now explained for the flexural deflection (bending), as this is the more demanding case (than torsion). The continuous beam is divided into n sections (like the wing) and each ith section is represented as a point mass m_i and a massless spring with stiffness k_i . The n mass-spring elements are connected in series to express the structural continuity of the beam. This discrete representation with n lumps allows considering flexural deflections for each lump as a function of time only. In other words, instead of $w = w(x, t)$, as in Eqn (1), we compute n functions $w_i(t)$ each of which corresponds to the spatial discretisation point (lump), $w_i(t) \approx w(x,t)\big|_{x=x_i}$.

Derivation of the stiffness coefficient k_i for each element was somewhat non-standard for the Eristalis wing; for $n = 3$ the stiffness matrix $\boldsymbol{K}$ is:

$$K = \left[\begin{array}{c:c} K_{11} & K_{12} \\ \hdashline K_{21} & K_{22} \end{array}\right] = \frac{2E}{l^3} \left[\begin{array}{c|c:c|c|c:c} 6a^{-3}I_1 + 6I_2 & -6I_2 & 0 & (3a^{-2}I_1 - 3I_2)l & -3I_2 l & 0 \\ \hline -6I_2 & 6I_2 + 6I_3 & -6I_3 & 3I_2 l & (3I_2 - 3I_3)l & -3I_3 l \\ 0 & -6I_3 & 6I_3 & 0 & 3I_3 l & 3I_3 l \\ \hdashline (3a^{-2}I_1 - 3I_2)l & 3I_2 l & 0 & (2a^{-1}I_1 + 2I_2)l^2 & I_2 l^2 & 0 \\ \hline -3I_2 l & (3I_2 - 3I_3)l & 3I_3 l & I_2 l^2 & (2I_2 + 2I_3)l^2 & I_3 l^2 \\ 0 & -3I_3 l & 3I_3 l & 0 & I_3 l^2 & 2I_3 l^2 \end{array}\right] \quad \text{Eqn (2)}$$

and has the characteristic tri-diagonal and block form. The wing was divided into elements of equal length $l = R/n$ except for the root element having length al. This division led to different masses m_i and area moments of inertia I_i for each section. The resulting lumped-parameter representation [34] is the system of n second-order ordinary differential equations (ODEs) $\boldsymbol{M}\ddot{\boldsymbol{w}} + \widetilde{\boldsymbol{K}}\boldsymbol{w} = \boldsymbol{F}$, where $\boldsymbol{M}$ is the mass matrix, $\boldsymbol{M}$ = diag[$m_1 \cdots m_n$], $\widetilde{\boldsymbol{K}}$ is the effective stiffness matrix, $\widetilde{\boldsymbol{K}} = -\boldsymbol{K}_{12}\boldsymbol{K}_{22}^{-1}\boldsymbol{K}_{21} + \boldsymbol{K}_{11}$, $\boldsymbol{w}$ is the vector of deflections at the lumps, $\boldsymbol{w}(t) = [w_1(t) \ldots w_n(t)]$ and $\boldsymbol{F}$ is the vector of external forces acting at the lumps, $\boldsymbol{F}(t) = [F_1(t) \ldots F_n(t)]$. Solutions of the ODEs are oscillatory and $n > (2r-1)\pi/\sqrt{\varepsilon}$ guarantees that the first r natural frequencies are accurate to ε per cent [35]. We chose $n = 20$, so that the accuracy of the first five frequencies was better than 2%, which we verified (in bending and torsion) for exact solutions of PDEs obtained by simplifying Eqn (1).

5.2.3 Aeroelastic Coupling

Aeroelastic coupling is achieved by solving the system of ODEs $\boldsymbol{M}\ddot{\boldsymbol{w}} + \widetilde{\boldsymbol{K}}\boldsymbol{w} = \boldsymbol{F}$ of the lumped parameter beam model above together with the integral equations of the aerodynamic model of Section 3. The aerodynamic force enters into $\boldsymbol{F}$, thus contributing to the wing deformations $\boldsymbol{w}$. These deformations $\boldsymbol{w}$ define a new shape of the wing which is fed into the aerodynamic model for computation of the aerodynamic force and so on in a continuous interaction.

5.2.4 Inertioelastic or Aeroelastic?

The coordinate system $x\ y\ z$ associated with the undeformed wing rotates through angles φ, θ, ψ with respect to the inertial system $X\ Y\ Z$. The bending deflections (u, v, w) refer to the displacements from the undeformed position (x, y, z), so that $X = X_0 + x + u$, $Y = Y_0 + y + v$, $Z = Z_0 + z + w$. Resolving the inertial system accelerations $\ddot{X}$, $\ddot{Y}$, $\ddot{Z}$ in the rotating frame $x\ y\ z$ and taking into account that the deflections $u = v = 0$, yields:

$$m\begin{bmatrix} \ddot{X} \\ \ddot{Y} \\ \ddot{Z} \end{bmatrix} = \begin{bmatrix} \text{Orientation} \\ \text{Matrix} \end{bmatrix} \times \underbrace{m\begin{bmatrix} -(\dot{\theta}^2 + \dot{\psi}^2)x \\ (\dot{\phi}\dot{\theta} + \ddot{\psi})x \\ (\dot{\phi}\dot{\psi} - \ddot{\theta})x \end{bmatrix}}_{F_1,\ \text{or applied force}} + \begin{bmatrix} \text{Orientation} \\ \text{Matrix} \end{bmatrix} \times \underbrace{m\begin{bmatrix} (\dot{\phi}\dot{\psi} + \ddot{\theta})w + 2\dot{\theta}\dot{w} \\ (\dot{\theta}\dot{\psi} - \ddot{\phi})w - 2\dot{\phi}\dot{w} \\ -(\dot{\phi}^2 + \dot{\theta}^2)w + \ddot{w} \end{bmatrix}}_{F_2,\ \text{or elastic response force}} \quad \text{Eqn (3)}$$

where $\boldsymbol{F}_1$ is generated by the insect's flight muscles while $\boldsymbol{F}_2$ is the wing elastic response (in bending) to both the applied force $\boldsymbol{F}_1$ and the aerodynamic force $\boldsymbol{A}$; both $\boldsymbol{F}_1$ and $\boldsymbol{F}_2$ are in the $x\ y\ z$ system. The question is which of the forces dominates in eliciting the elastic response $\boldsymbol{F}_2$: the applied force $\boldsymbol{F}_1$ or the aerodynamic force $\boldsymbol{A}$? This question can be answered from Eqn (3) if the wing mass m, wing kinematics φ, θ, ψ and wing deflections w are known together with the corresponding aerodynamic force $\boldsymbol{A}$.

The aeroelastic model described above takes as input the wing kinematics, mass, geometry and material properties and outputs the deflections w and the aerodynamic force $\boldsymbol{A}$. It is an engineering design tool for insect-like flapping-wing micro air vehicles allowing prediction of the wing behaviour for the input data assumed for the design. The model can also be used to analyse the insect wing, provided the required input data, e.g. E and I needed in Eqn (2), are known reliably. However, the reported values of E and I for insect wings vary widely [36][37]. An alternative approach, adopted here, makes use of the deflection data produced in this project combined with the aerodynamic model of Section 3. Using the measured data for

the kinematics θ, φ, ψ and wing deflections w, the forces $\boldsymbol{F}_1$ and $\boldsymbol{F}_2$ are computed from Eqn (3). The aerodynamic force $\boldsymbol{A}$, corresponding to these measured kinematic and deflection data, is calculated using the aerodynamic model of Section 3. The forces thus obtained $\boldsymbol{F}_1$, $\boldsymbol{F}_2$ and $\boldsymbol{A}$ are compared in Figure 6 showing that overall $F_{1,\mathrm{rms}}$ dominates compared with A_{rms}, for bending.

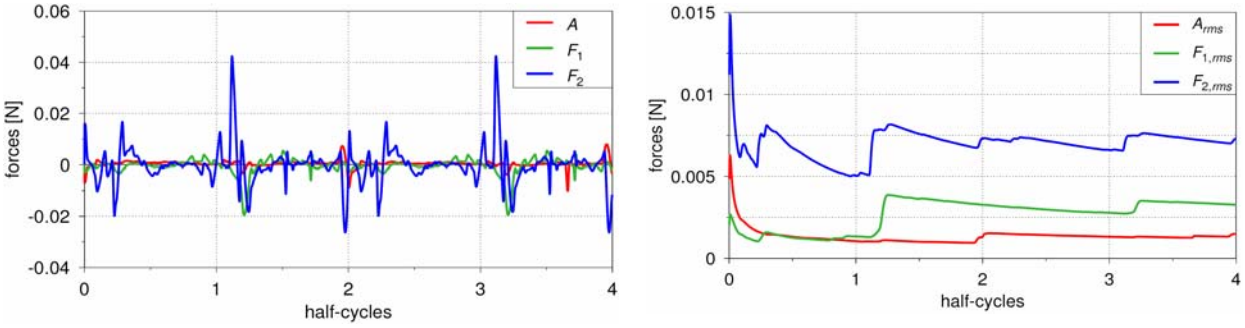

Figure 6: Instantaneous values of F_1, F_2 and A for two flapping cycles from Eqn (3) and the aerodynamic model of Section 3, left. Progressive average magnitudes calculated as RMS values using $F_{\mathrm{rms}}(t) = \sqrt{\{(1/t)\int_0^t |F(\tau)|^2 \,\mathrm{d}\tau\}}$, right. These show that, for bending, during the first half-cycle (start-up) $F_{1,\mathrm{rms}}$ and A_{rms} are comparable. Thereafter $F_{1,\mathrm{rms}}$ dominates with $F_{1,\mathrm{rms}}/A_{\mathrm{rms}} \approx 2$.

6.0 SENSOR-RICH FEEDBACK CONTROL

As described earlier, obstacle-avoidance is central to indoor flight. While providing an efficient platform with high aerodynamic performance, a flapping-wing vehicle poses significant challenges in terms of positional awareness, flight stability and robustness against disturbances or changes. This requires a complex flight control system, and here again the solution can be found in insect flight [38]. In modern aircraft, flight dynamics are governed by a few *complex* controllers fed by a small number of sensors. The computational overhead is significant. Flight dynamics for insects are as complex (if not more so) and they must, therefore, solve similarly complex equations. We hypothesise that in insects, however, the required information is generated by favouring measurement rather than computation — a large number of sensors feed many *simple* controllers. Biological evidence substantiates this claim. For a fly, for example, of the 338000 neurons, only about 1% form part of the central processing complex in the brain [39]; the remainder are all simple sensor-processing neurons. This indicates a low computational overhead, and is made possible not by solving the complex equations but by the insect 'knowing' these few solutions. We study the implications of this sensor-rich platform and open a new avenue of multidisciplinary research on reverse-engineering of insect flight for micro air vehicle applications. Emulating an insect-like platform will require a multitude of sensors which, in turn, will call for multi-sensor data fusion. In fact, a much broader synergy of flight mechanics and control systems is required for a successful design.

7.0 CONCLUSIONS

This paper has discussed on-going research by the authors, aimed at the development of a flapping-wing micro air vehicle based on insect-like aerodynamics. From biological research the aerodynamic phenomena encountered in hover are now reasonably well understood and these have been described. We have outlined our aerodynamic model for flapping wings, which is quasi-three-dimensional but predicts measured force vs time histories very well for a 3D wing. Reynolds-Averaged Navier Stokes modelling of wings at high angles of attack has shown the importance of spanwise flow in stabilising the LEV. Although Kelvin-Helmholtz Instabilities occur in leading and trailing-edge vortex sheets as Reynolds

Number is increased, this does not cause the detachment of the LEV, so lift is maintained.

New experimental results on insect wing deflections in flight have been presented. These have allowed us to develop an aeroelastic model of flapping wings, using input from our aerodynamic model. With this model and the measured wing deflections we have been able to address the relative significance of inertioelastic and aeroelastic bending.

Finally, some thoughts have been offered on a potential way forward for flight control of an insect-inspired FMAV – sensor-rich feedback control.

ACKNOWLEDGEMENTS

The authors gratefully acknowledge the support of the Engineering and Physical Sciences Research Council and the Ministry of Defence Joint Grant Scheme: work presented here has been partly supported by grants GR/M78472, GR/M22970 & GR/S23025/01. The aeroelastic experimental work reported here was conducted by Mr Simon Walker, Dr Graham Taylor and Prof Adrian Thomas of Oxford University, Department of Zoology, with input on optical metrology techniques from Dr Iain Wallace and Dr Andrew Moore of Heriot-Watt University.

REFERENCES

[1] R. Zbikowski, Flapping Wing Autonomous Micro Air Vehicles: Research Programme Outline, in *14th Int. Conf. on Unmanned Air Vehicle Systems*, vol. Supplementary Papers, 1999, pp. 38.1–38.5.

[2] R. Zbikowski, Flapping Wing Micro Air Vehicle: A Guided Platform for Microsensors, in *RAeS Conf. on Nanotechnology and Microengineering for Future Guided Weapons*, 1999, pp. 1.1–1.11.

[3] R. Zbikowski, Flapping Wing Technology, in *European Military Rotorcraft Symposium*, Shrivenham, UK, 21-23 March 2000, pp. 1–7.

[4] R. Dudley, *Biomechanics (Structures & Systems): A Practical Approach*, OUP, 1992.

[5] R. Zbikowski, C B Pedersen, S A Ansari & C Galinski, Flapping Wing Micro Air Vehicles, *Lecture Series: Low Reynolds Number Aerodynamics on Aircraft Including Applications in Emerging UAV Technology*, RTO/AVT 104, von Karman Institute, Belgium, 2003.

[6] M. I. Woods, J. F. Henderson, and G. D. Lock, Energy Requirements for the Flight of Micro Air Vehicles, *Aeronautical Journal*, **105**:135-149, 2001.

[7] C. P. Ellington, The Aerodynamics of Hovering Insect Flight: III. Kinematics, *Philosophical Transactions of the Royal Society of London Series B*, **305**:41–78, 1984.

[8] A. R. Ennos, The Kinematics and Aerodynamics of the Free Flight of Some Diptera, *Journal of Experimental Biology*, **142**:49–85, 1989.

[9] M. H. Dickinson, F.-O. Lehmann & S. P. Sane, Wing Rotation and the Aerodynamic Basis of Insect Flight, *Science*, **284**:1954–1960, 1999.

[10] R. Zbikowski, On Aerodynamic Modelling of an Insect-like Flapping Wing in Hover for Micro Air Vehicles, *Philosophical Transactions of the Royal Society of London Series A*, **360**:273–290, 2002.

[11] C. P. Ellington, C. van den Berg, A. P. Willmott & A. L. R. Thomas, Leading-edge Vortices in Insect Flight, *Nature*, **384**:626–630, 1996.

[12] H. Liu, C. P. Ellington, , K. Kawachi, , C. van den Berg, , & A. P. Wilmott, A Computational Fluid Dynamic Study of Hawkmoth Hovering, *Journal of Experimental Biology*, **201**:461–477, 1998.

[13] S. A. Ansari, *A Nonlinear, Unsteady, Aerodynamic Model for Insect-like Flapping Wings in the Hover with Micro Air Vehicle Applications*, PhD thesis, Department of Aerospace, Power and Sensors, Cranfield University, Shrivenham, 2004.

[14] S.A. Ansari, R. Zbikowski, and K. Knowles, Aerodynamic Modelling of Insect-like Flapping Flight for Micro Air Vehicles, *Progress in Aerospace Sciences*, **42** (2): 129-172, 2006.

[15] S.A. Ansari, R. Zbikowski & K. Knowles, A Nonlinear Unsteady Aerodynamic Model for Insect-like Flapping Wings in the Hover: Part I. Methodology and Analysis, *Proceedings IMechE Part G: Journal of Aerospace Engineering*, **220** (G2):61-83, 2006.

[16] S.A. Ansari, R. Zbikowski & K. Knowles, A Nonlinear Unsteady Aerodynamic Model for Insect-like Flapping Wings in the Hover: Part II. Implementation and Validation, *Proceedings IMechE Part G: Journal of Aerospace Engineering*, **220** (G3):169-186, 2006.

[17] S.A. Ansari, K. Knowles & R. Zbikowski, Design Guidelines for Flapping-Wing Micro UAVs, *Int. Powered Lift Conf.*, Grapevine, TX, 3-6 October 2005. Pub: SAE Paper no 2005-01-3197.

[18] W. Thomson (Lord Kelvin), On Vortex Motion, In *Mathematical and Physical Papers: Volume IV Hydrodynamics and General Dynamics*. Cambridge University Press, 1910.

[19] M. H. Dickinson & K. G. Götz, Unsteady Aerodynamic Performance of Model Wings at Low Reynolds Numbers, *Journal of Experimental Biology*, **174**: 45–64, 1993.

[20] C. van den Berg, & C. P. Ellington, The Three-Dimensional Leading-Edge Vortex of a "Hovering" Model Hawkmoth, *Philosophical Transactions of the Royal Society of London Series B*, **352** (1351): 329–340, 1997.

[21] P.C. Wilkins, K. Knowles & R. Zbikowski, CFD Investigation of Flapping-wing Micro Air Vehicle Aerodynamics, *European Micro Air Vehicle Conf.*, Braunschweig, Germany, 25 - 26 July 2006.

[22] A. P. Willmott, C. P. Ellington, and A. L. R. Thomas, Flow visualization and unsteady aerodynamics in the flight of the Hawkmoth, Manduca sexta, *Philosophical Transactions of the Royal Society of London B*, **352**:303-316, 1997.

[23] J. M. Birch and M. H. Dickinson, Spanwise Flow and the Attachment of the Leading-Edge Vortex on Insect Wings, *Nature*, **412**:729–733, 2001.

[24] M. Ramasamy and J. G. Leishman, Phase-Locked Particle Image Velocimetry Measurements of a Flapping Wing, *Journal of Aircraft*, **43** (6): 1867-1875, 2006.

[25] L. J. Zeng, H. Matsumoto, and K. Kawachi. A fringe shadow method for measuring flapping angle and torsional angle of a dragonfly wing, *Measurement Science and Technology*, 7(5):776–781, 1996.

[26] A. P. Willmott and C. P. Ellington. Measuring the angle of attack of beating insect wings: Robust three-dimensional reconstruction from two-dimensional images. *Journal of Experimental Biology*,

200(21):2693–2704, 1997.

[27] H. Wang, L. J. Zeng, and C. Y. Yin. Measuring the body position, attitude and wing deformation of a free-flight dragonfly by combining a comb fringe pattern with sign points on the wing. *Measurement Science Technology*, 13(6):903–908, 2002.

[28] T. L. Daniel and S. A. Combes. Flexible wings and fins: Bending by inertial or fluid-dynamic forces? *Integrative and Comparative Biology*, 42(5):1044–1049, 2002.

[29] R. J. Wootton, R. C. Herbert, P. G. Young, and K. E. Evans. Approaches to the structural modelling of insect wings. *Philosophical Transactions of the Royal Society B: Biological Sciences*, 358(1437):1577–1587, 2003.

[30] I.Wallace, N. J. Lawson, A. R. Harvey, J. D. C. Jones, and A. J. Moore. High-speed photogrammetry system for measuring the kinematics of insect wings. *Applied Optics*, 45(17):4165–4173, 2006.

[31] R. L. Bisplinghoff, H. Ashley, and R. L. Halfman. *Aeroelasticity*. Addison-Wesley, Reading, MA, 1955.

[32] D. C. Kammer and A. L. Schlack, Jr. Dynamic response of a radial beam with nonconstant angular velocity. *Transactions of the ASME: Journal of Vibration, Acoustics, Stress, and Reliability in Design*, 109(2):138–143, 1987.

[33] W. D. Pilkey. *Formulas for Stress, Strain and Structural Matrices*. Wiley, Hoboken, NJ, 2nd edition, 2005.

[34] S. K. Tolani and R. D. Rocke. A strain energy comparison of discrete modeling for vibrating continuous systems. *Journal of Engineering for Industry*, 94(1):23–30, 1972.

[35] R. E. D. Bishop, G. M. L. Gladwell, and S. Michaelson. *The Matrix Analysis of Vibration*. Cambridge University Press, Cambridge, 1965.

[36] S. A. Combes and T. L. Daniel. Flexural stiffness in insect wings II. Spatial distribution and dynamic wing bending. *Journal of Experimental Biology*, 206(17):2989–2997, 2003.

[37] F. Song, K. L. Lee, A. K. Soh, F. Zhu, and Y. L. Bai. Experimental studies of the material properties of the forewing of cicada (Homoptera, Cicadidae). *Journal of Experimental Biology*, 207(17):3035–3042, 2004.

[38] R. Zbikowski, Sensor-Rich Feedback Control, *IEEE Instrumentation & Measurement Magazine*, 19–26, 2004.

[39] N. J. Strausfeld, *Atlas of an Insect Brain.* Springer-Verlag, Berlin and New York, 1976.